Applied Thermal Engineering 267 (2025) 125697

Contents lists available at ScienceDirect

Applied Thermal Engineering

journal homepage: www.elsevier.com/locate/apthermeng

Research Paper

The impact of TCMs in TES systems with PCMs: Modelling and dynamic simulation of a novel prototype

Silvia Cesari [a,*], Giuseppe Emmi [b], Michele Bottarelli [a]

[a] Department of Architecture, University of Ferrara, Via Quartieri 8, Ferrara 44121, Italy
[b] Department of Architecture and Arts, University IUAV of Venice, Dorsoduro 2206, Venezia 30123, Italy

ARTICLE INFO

Keywords:
Thermochemical materials (TCMs)
Phase change materials (PCMs)
Thermal energy storage (TES)
Dynamic simulation
TRNSYS
Coefficient of performance (COP)

ABSTRACT

Among sensible, latent and thermochemical thermal energy storage (TES), thermochemical materials (TCMs) result to be the most promising solution to achieve EU target for 2050 of net-zero GHG emissions. A novel TES solution using TCMs and phase change materials (PCMs) for space heating and cooling is being developed within the Horizon Europe project ECHO. A TRNSYS model able to simulate the prototype in dynamic mode at system scale was created to optimise the installation and testing of the prototype. Experimental data from a small set-up of the reactor were used to define the equations describing the charging and discharging phases of TCM, which were implemented in the reactor model. The ability of TCM to increase the efficiency of the system where it is adopted was investigated for the heating period. The TCM-integrated heat pump system showed an 8.8 % reduction in seasonal electricity consumption compared to the system without TCM, and an increase in the seasonal COP from 3.4 to 3.8. Finally, the evaluation of the thermal contribution provided by TCM combined with PCM highlighted that the two TES systems were able to cover about 10 % of the heating energy demand, with PCM accounting for almost 50 % of the TCM contribution.

1. Introduction

The EU Green Deal aims for a 100 % reduction of GHG emissions by 2050 [1]. Within this framework, thermal energy storage (TES) systems play a pivotal role in achieving EU objective. TES technology fosters the exploitation of renewable energy sources, thus reducing reliance on fossil fuels and mitigating environmental impacts. TES systems allow to store excess thermal energy during off-peak periods of energy demand and release it in peak-time, thereby improving energy efficiency and enabling the integration of intermittent renewable energy sources [2,3].

Among TES technologies, thermochemical materials (TCMs) and phase change materials (PCMs) represent two cutting-edge approaches with distinct operational characteristics. The former have attracted increasing attention for their superior energy density and long-term storage potential, particularly in applications requiring seasonal thermal storage [4]. The energy storage process in TCMs is governed by endothermic and exothermic reactions, typically involving hydration-dehydration cycles, which can be tailored to operate at different temperature ranges suitable for building applications [5]. Studies have demonstrated the feasibility of TCMs in solar energy storage systems, where they can store thermal energy during sunny periods and release it during cloudy or nighttime conditions [6], as well as for the utilisation of industrial waste heat [7]. The performance of TCMs is highly dependent on the choice of material, the synthesis procedure and the design of the reactor, with current research focusing on optimising these parameters to improve reaction kinetics, thermal management, and system efficiency [8,9].

Differently, PCMs use the latent heat of phase transition, typically from solid to liquid and viceversa, to store and release thermal energy at nearly constant temperatures. For this reason, PCMs are widely adopted in water storage applications, as well as in solar systems, where they allow to significantly increase solar thermal energy storage capacity, thereby reducing the supply–demand gap and increasing the exploitation of solar energy [10–12]. Owing to their ability to maintain stable temperatures during phase transition, PCMs are also widely integrated in space heating and cooling systems, where thermal comfort and energy efficiency are critical factors [13,14]. PCMs integrated in radiant floor systems can shave peak loads and shift energy consumption from high-demand to low-demand hours, when pricing is lower. During the day in winter, PCM can store the available renewable heating loads, and subsequently emit them at comfort temperature in the night; in summer, PCMs are able to ensure sufficient thermal resilience to absorb thermal loads. Then, these loads are released in the night when outdoor

* Corresponding author.
E-mail address: silvia.cesari@unife.it (S. Cesari).

https://doi.org/10.1016/j.applthermaleng.2025.125697
Received 7 September 2024; Received in revised form 4 January 2025; Accepted 21 January 2025
Available online 27 January 2025

Nomenclature

Acronyms

AHU	air handling unit
CC	cooling coil
CHS	charging control strategy
COP	coefficient of performance [-]
$\overline{COP}$	average coefficient of performance [-]
CSP	concentrated solar power
deHUM-CC	dehumidification and cooling coil
F	fan
EL-HC	electrical heating coil
HEX	heat exchanger
HGHE	horizontal ground heat exchanger
HP	heat pump
HRU	heat recovery unit
HUM	humidifier
LTMH	low-temperature metal hydride
PCM	phase change material
PCM_c	coil of PCM tank
PV/T	photovoltaic/thermal collector
pm	power modulation
R	TCM reactor
SoC	state of charge
SSTES	seasonal solar thermal energy storage
TCM	thermochemical material
TES	thermal energy storage
UT	user tank

Symbols

c_p	specific heat [kJ/(kg·K)]
E	energy [kWh] or [kJ]
H_{SL}	latent heat [kJ/kg]
J	enthalpy [kJ/kg]
m	mass [kg]
$\dot{m}$	mass flow rate [kg/h]
$\dot{q}$	specific thermal power [W/(kg_{TCM})]
$\dot{Q}$	thermal or electric power [W]
$\dot{R}$	adsorption/desorption rate [g/h]
$\dot{r}$	specific adsorption/desorption rate [g/(h·kg_{TCM})]
T	temperature [K]
X	humidity ratio [g/kg]

Greek Symbols

Δ	difference [-]
η	efficiency [%]
λ	thermal conductivity [W/(m·K)]
ρ	density [kg/m^3]

Subscripts

cond	condenser
dis	discharging
evap	evaporation
el	electrical
hum	humidification
in	inlet
max	maximum
out	outlet
t	time t
t_0	time previous to time t
th	thermal
w	water

temperatures usually drop, thus pre-cooling the floor and reducing the cooling demand for the following day [15–18]. Furthermore, the integration of PCMs in components of the building envelope, such as walls and roofs, has been explored to smooth indoor temperature fluctuations and reduce heating and cooling loads [19–22]. Advancements in PCM technology have largely focused on enhancing thermal conductivity by means of metal foams or additives, improving cycling stability, and developing effective encapsulation techniques to avoid leakage and degradation issues [23,24]. A modified structure of metal foam with gradient porosity of three stratification layers was investigated by Zhuang et al. [25] to optimise the melting characteristic of composite PCMs. Again, metal foam was considered in Ref. [26] to analyse the melting performance of magnetic nano-enhanced PCMs embedded in metal foam subjected to a non-uniform magnetic field. Among the most recent innovative research there is the use of ultrasonic and magnetic field to significantly reduce the melting time of hybrid nano-enhanced PCMs, strongly increase TES efficiency as well as their energy storage amount [27]. Innovative research, applications and advancements about PCMs include a huge amount of works. Nevertheless, as the primary objective of this study is evaluating the impact of TCM in TES systems already incorporating PCMs – not innovating in PCMs – current experimental research on innovative PCM solutions was not included, focusing instead on the best commercially available standard PCM option to be used in the system. For this reason, and for the sake of brevity, a thorough and extensive review of current experimental research on innovative PCM solutions has not been included in this section.

Against this background, the integration of TCMs and PCMs in TES systems represents a promising solution to provide space heating and cooling by capitalising on the complementary properties of these materials with the aim to maximally exploit renewable energy sources. For this reason, recent advancements have highlighted the need for numerical models that can accurately simulate the dynamic behaviour and system-scale performance of integrated TES systems [28,29]. Modelling TCMs and PCMs in dynamic mode allows for a more reliable representation of the system in actual conditions. The dynamic response of TES systems is affected by various factors, including fluctuating thermal loads, material interactions, and external conditions. The reversible chemical reactions in TCMs are influenced by temperature, pressure, and material properties, all of which vary over time, thus requiring accurate models able to simulate these complexities faithfully under dynamic conditions. Moreover, the integration of TCMs with PCMs in hybrid systems introduces additional layers of interaction, as the materials operate both together and with all the other components of the system according to different principles, under various conditions and timescales. Therefore, comprehensive system-scale models are essential to account for these interactions, assess the overall system performance, and define optimised and efficient control strategies for practical applications [5].

Nevertheless, review of the literature has uncovered a critical knowledge gap in the development of dynamic models and simulations of TES systems incorporating both TCMs and PCMs. While several studies have numerically and dynamically analysed PCMs, the integration of PCMs with other TES technologies, such as TCMs, remains largely unexplored [30–32]. As for TCMs, their dynamic behaviour has been rarely investigated. Existing studies have primarily focused on the performance of TCMs under steady-state conditions. When dynamic analysis was carried out, the TCM system was exclusively examined – without taking into account other TES systems – in extremely simplified configurations. Indeed, the majority of the works investigated the system merely at the TCM reactor level or by considering only a few components, thus neglecting the dynamic interactions within the whole system. The dynamic desorption process of a TCM reactor was analysed

by Xu et al. [33] through a 2D numerical model; similarly, optimised conditions for the charging process of a TCM system were investigated with a COMSOL model, highlighting that the use of an electrical heater allowed to achieve full material charging [34]. Again, the impact of different conditions – such as porosity, temperature, pressure, flow rate and thermal conductivity – on the hydration process in a TCM reactor was studied by using a multi-physics model. Low thermal conductivity of solid phase was identified as the most important factor which limits the reaction [35]. Differently from the studies mentioned above, which were focused exclusively on the TCM reactor, Zeng et al. [36] considered different integration strategies of open-cycle TCM reactors with HVAC systems and developed a 1D model to simulate their thermal performance across diverse buildings and climates, especially for space heating. The model was then validated by experimental data. An open-cycle TCM reactor used for space heating was also analysed by Zhang et al. [37]. However, in this case the TCM reactor was integrated with an internal water-to-air microchannel tube heat exchanger (HEX), and an external air-to-air heat recovery unit (HRU). Different TCM system configurations were numerically compared through a COMSOL model. In a previous work, Zhang et al. [38] investigated the impact of adding a PV/T collector and heat exchanger HEX on the performance of the TCM system for space heating using COMSOL too. The integration of TCMs in solar-driven systems has been examined in several studies. The adoption of different TCMs in a seasonal solar thermal energy storage (SSTES) system destined for residential heating was explored by Ma et al. [39]. The dynamic charging and discharging performance of the SSTES was simulated using actual weather data, solar thermal collector models, domestic heating demand models, and chemisorption models. Similarly, a SSTES system incorporating seasonal and cascade TES using TCMs for space heating was analysed by Yue et al. [40]. Again, the processes of charging and discharging a closed-type TCM reactor integrated with solar collectors and an electric boiler for space heating of a residential building was studied by Mikos-Nuszkiewicz et al. [41]. The model used to conduct the analysis was an intermediate approach between lumped-element models and 2D/3D spatially resolved models. In addition, a novel hybrid TCM system designed to harness ultra-low-grade solar heat in cold regions was numerically examined by Jiang et al. [42]. The integration with a water-based PV/T system allowed to achieve significant increase in energy efficiency.

Nevertheless, all the studies reviewed above exclusively considered TCMs not integrated with other TES technologies such as PCMs. Only a very small number of works have attempted to model TES systems combining TCMs and PCMs in a dynamic mode at the system scale, thus incorporating both the reactor and auxiliary devices such as heat exchangers, heat pumps, thermal storage tanks, etc. A concentrated solar power (CSP) plant integrated with a hybrid TES unit that combines thermochemical and latent heat storage techniques was investigated by Mellouli et al. [43]. The thermochemical heat released by the low-temperature metal hydride (LTMH) tank was stored as latent heat in a PCM truncated heat exchanger for reuse during desorption process. The performance of the MH/PCM-TES unit was analysed through a two-dimensional mathematical model and a numerical code written in Fortran-90. Results demonstrated that the use of PCM allowed to achieve a 30 % increase in the energy recovery efficiency of the hybrid heat storage unit. Furthermore, it was found that PCM thermo-physical properties and operating temperatures had a substantial effect on the system performance. The same MH/PCM-TES unit was considered to conduct a comparative analysis between a reference configuration using only TCM and two different PCM heat exchanger configurations. Again, a bidimensional mathematical model and a numerical code written in Fortran-90 were adopted to predict the dynamic behaviour of the three storage systems [44]. Finally, a solar-driven thermal system integrated with TCM and PCM storage units to provide heating and cooling was investigated by Zisopoulos et al. [45]. A thermodynamic model of the system composed of PV/T collectors and flat plate solar collectors coupled with TCM and PCMs units was developed in Aspen Plus Dynamics and integrated with Matlab/Simulink. Dynamic simulations showed that the system was able to cover the building heating demand at an average minimum rate of 81 % and maximum of 93 %.

Against this background, a novel TES solution exploiting TCMs and PCMs to provide space heating and cooling is being developed within the Horizon Europe project ECHO [46]. A lab-scale prototype will be installed at the TekneHub lab of the University of Ferrara, Italy. With the aim to support and optimise the realisation and testing of the prototype, as well as to sustain the definition of the control system, a TRNSYS model of the ECHO plant was developed. The model and the analysis of the impact of TCM in TES systems incorporating PCMs were developed by addressing the following research questions:

- Can TCMs be effectively combined with PCMs and integrated in TES systems to capitalise on the complementary properties of these materials and maximise the exploitation of renewable energy sources?
- Is it possible to accurately simulate the dynamic behaviour and system-scale performance of integrated TES systems using TCMs and PCMs?
- Which parameters can be considered as control parameters and stopping criteria to effectively define the control algorithm of the model?
- How much TCM is able to increase the efficiency of the system where it is integrated?
- Which is the thermal contribution provided by the two TES systems, TCM and PCM?

The main novelty of the work regards the complexity of the system modelled and the method adopted. Considering the complexity, the primary contribution of the research lies in the development of a dynamic model that integrates TCMs and PCMs in a TES system to provide space heating and cooling. Therefore, the developed TRNSYS model represents a significant advancement over existing studies by incorporating the complex interactions between TCMs and PCMs, thus providing a more accurate depiction of the system behaviour under realistic operating conditions. Furthermore, the contribution of the work also consists in the inclusion of a closed-loop TCM reactor, which has been rarely modelled in transient mode and at system scale. Additionally, the present study addresses the critical need for system-scale models that incorporate auxiliary devices, such as humidifiers, heat exchangers, thermal storage tanks, heat pumps, heating and cooling coils, etc., alongside the TES materials. Finally, by capturing the full dynamics of the TES system, the model offers valuable insights into the design and optimisation of integrated TES solutions for building applications.

The findings of the present work are expected to contribute to the broader understanding of integrated TES technologies and support the development of more efficient and sustainable energy storage solutions for the building sector.

2. Methodology

The prototype of the ECHO system that will be installed in a mock-up building in Ferrara, Italy, and on which the TRNSYS model was developed is firstly described. The system layout, the operating modes, the components and their role are explained. Secondly, the development of the TRNSYS model and its preliminary validation are illustrated. Finally, the analysis conducted via simulations was reported. Optimal TCM quantity to efficiently meet the building heating demand, different charging control strategies (CHS), and the equivalent coefficient of performance (COP) of the TCM integrated system versus a common heat pump were investigated, along with the contribution of the two TES systems, TCM and PCM.

2.1. ECHO system prototype

The ECHO system is composed of an air loop and a water loop, which is aimed to couple the air loop with the heat pump. The air loop is designed with a layout similar to a conventional air handling unit structure, as illustrated in Fig. 1. It includes the TCM reactor, the cooling coil, the fan, the heat recovery unit, the humidifier, the dehumidification and cooling coil, the air-to-water heat exchanger connected to the PCM tank, the heating coil and the electrical heating coil. The intermediate water loop allows an easier regulation of the heat pump, a higher flexibility in the control strategy, a major reliability of the system and an easier maintenance. The water loop includes several tanks: the user tank; the PCM tank that is used to preheat the airflow at the inlet of the heat recovery unit during the discharging mode; the high-temperature storage tank at the outlet of the heat pump condenser; the cold storage one that is used as heat source for the evaporator.

The main operating modes of the ECHO system are the discharging (or heating mode) and the charging. During the discharging mode (Fig. 2), the following devices operate:

- the reactor, where humid air flowing through the TCM hydrates it, and it is then dehumidified and heated (phase 1-2 in Fig. 2);
- the cooling coil, which allows that the heat generated is exploited through the hydronic loop and provided to the user (phase 2-3);
- the fan, used to overcome the pressure drops inside the circuit and ensure the airflow rate (phase 3-4);
- the heat recovery unit (phase 4-5 and 8-9);
- the ultrasonic humidifier, aimed to reintegrate the water content adsorbed in the reactor during the charging mode (phase 5-6);
- the air-to-water heat exchanger, which is used to release the heat from the PCM storage tank (phase 7-8).

Differently, the following components operate during the charging mode (Fig. 3):

- the reactor, inside which the overheated and dry air dehydrates the TCM (phase 1-2 in Fig. 3);
- the fan (phase 3-4) and the heat recovery unit (phase 4-5 and 8-9);
- the dehumidification and cooling coil linked to the cold storage tank, where the heat pump evaporator extracts heat (phase 6-7);
- the heating coil that releases heat to the high-temperature tank (phase 9-10). The extra amount of heat that otherwise would have to be rejected into the ambient is used to charge the PCM tank or the user storage tank;
- the auxiliary electric heater to increase the temperature at the inlet of the reactor (phase 10-11).

2.2. TRNSYS model

The model of the ECHO system developed in TRNSYS included the main components of the plant, that is, the TCM reactor, the cooling coil, the fan, the heat recovery unit, the humidifier, the dehumidification and cooling coil, the pre-heating coil (connected to the PCM tank), the heating coil and the electrical heating coil, as illustrated in Fig. 4. Furthermore, also the heat pump and the user tank were included in the model. As already mentioned before, different devices work according to the operating mode.

Standard types and one non-standard type, i.e. Type 840 for the PCM-integrated storage tank, were used to simulate all the components, except for the TCM reactor.

As regards the PCM to be included in the tank, a lab-scale set-up of the TES system had been created and experimental tests have been carried out to investigate the thermal performance of macro-encapsulated paraffin PCM and hydrated salts under charge/discharge cycles. Both the organic and inorganic PCMs, identified as A32 and S32 [47], respectively, were provided by PCM Products Ltd [48], partner of ECHO project. Thermophysical properties of the PCMs analysed are reported in Table 1; properties of the selected PCM were used to define the external file called by Type 840. Despite its lower thermal conductivity and latent heat, thereby the ability to develop smaller thermal powers with the same system geometry compared to hydrated salts, the paraffin PCM A32 resulted to be the best option to build the required TES system. Experimental results under charge/discharge cycles highlighted its long-term stability, the lack of undercooling, and non-corrosiveness. In addition, further experimental tests are being conducted to enhance its low thermal conductivity by means of metal foams. However, taking into account the primary objective of this study – evaluating the impact of TCM in TES systems by incorporating PCMs – and for the sake of brevity, current experimental research on innovative PCM solutions was not included, focusing instead on the best commercially available standard PCM option.

Considering the TCM reactor, experimental tests had been previously conducted on a lab-scale set-up of the reactor working with $CaCl_2$ impregnated into porous vermiculite. The collected experimental data regarding the maximum specific thermal power $\dot{q}_{max}$ [W/kg$_{TCM}$] and the

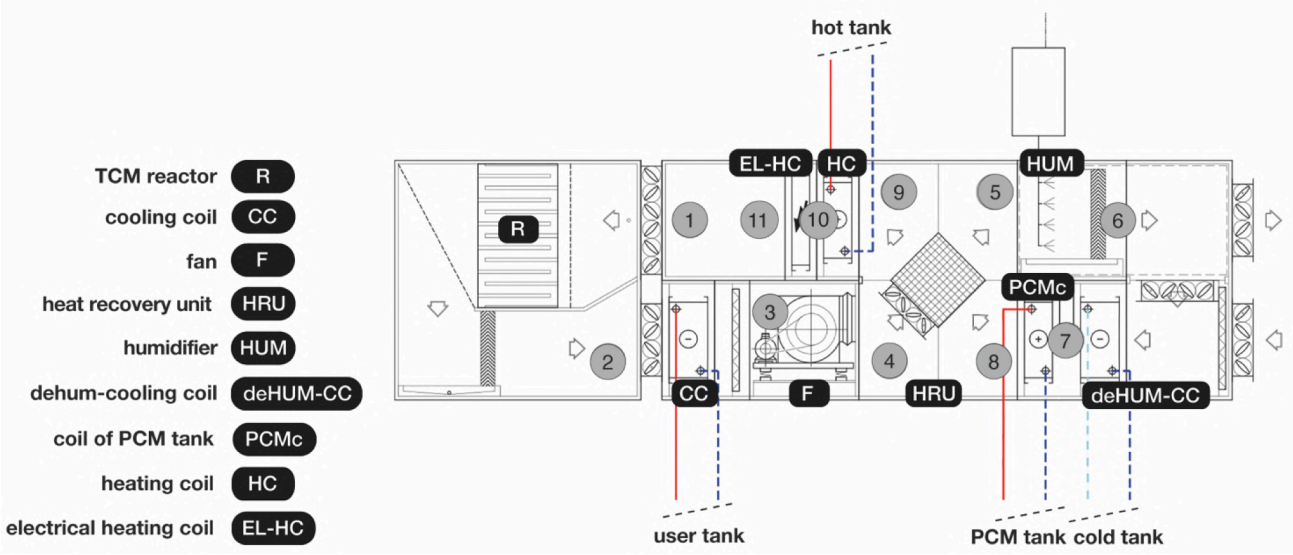

Fig. 1. The air handling unit section design of the ECHO prototype.

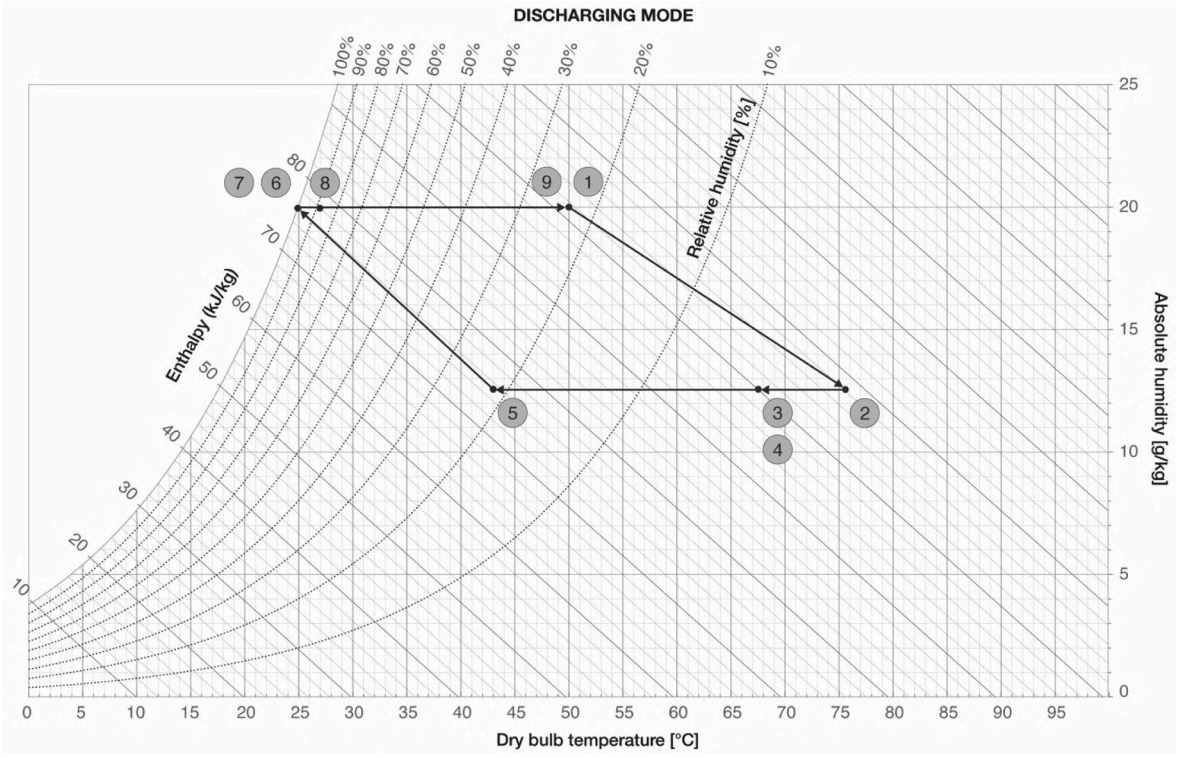

Fig. 2. Psychrometric conditions in discharging mode.

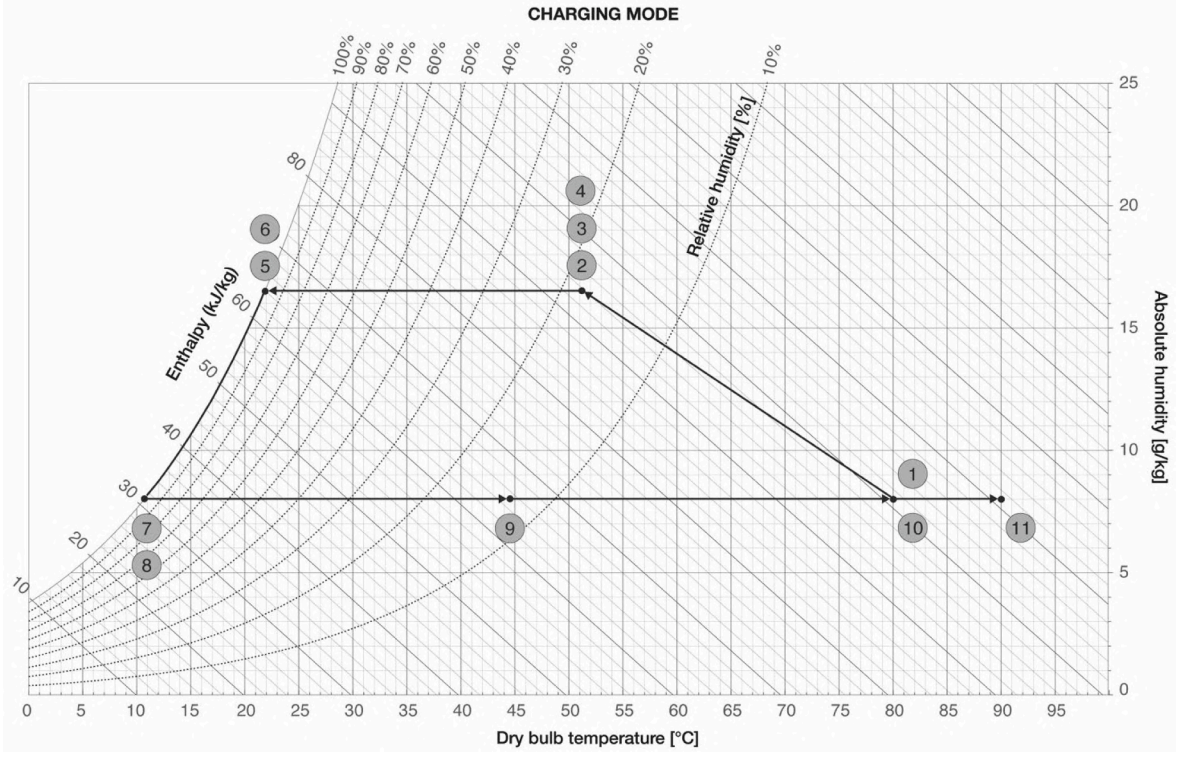

Fig. 3. Psychrometric conditions in charging mode.

maximum specific adsorption or desorption rate $\dot{r}_{max}$ [g/(h·kg$_{TCM}$)] were used to define the equations describing the charging and discharging phases of TCM. The maximum water mass $m_{w_{max}}$ [g] adsorbed or desorbed in the period t_{max} [h] was also considered. The reactor was then modelled in TRNSYS as a black box governed by a system of equations including those mentioned before, which were able to provide the most relevant data of the working reactor for each timestep, thus allowing to properly operate and optimise the other components of the system. Average experimental and assumed values for parameters used in simulations are reported in Table 2.

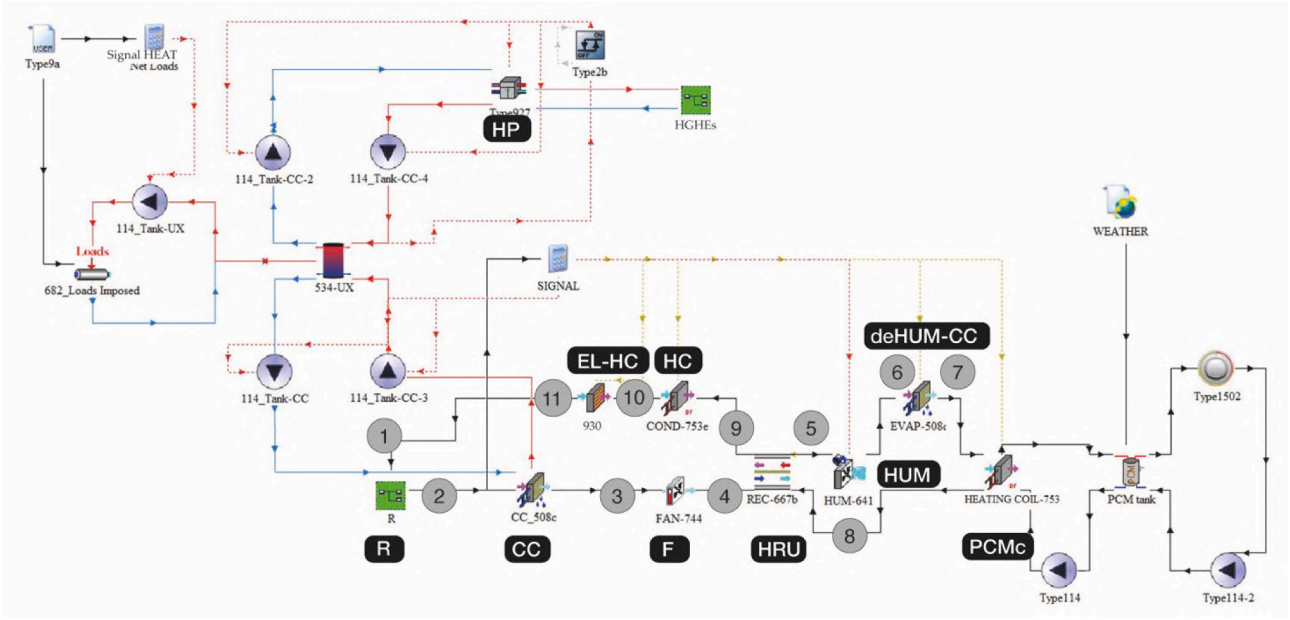

Fig. 4. TRNSYS model of the ECHO system.

Table 1
Thermophysical properties of A32 and S32 [47].

PCM	Melting point [°C]	ρ [kg/m^3]	H_{SL} [kJ/kg]	c_p kJ/(kg·K)	λ W/(m·K)
A32	32	845	120	2.2	0.21
S32	32	1460	220	1.9	0.51

Table 2
Parameters used in simulations.

Operating mode	$\dot{q}_{max}$ [W/kg$_{TCM}$]	$\dot{r}_{max}$ [g/(h·kg$_{TCM}$)]	$m_{w_{max}}$ [g]
Discharging	65	207	0.97 ·m_{TCM}
Charging	65	69	0.97 ·m_{TCM}

The relevant equations describing the charging and discharging phases of TCM and used to simulate the thermal performance of the TCM reactor are reported below. A *SIGNAL* parameter was identified to define three main operation modes of the TCM reactor: discharging (*SIGNAL* = -1), charging (*SIGNAL* = 1) and standby (*SIGNAL* = 0). The *SIGNAL* parameter was evaluated as:

$$SIGNAL = EQL(SIGNAL\_EXT, 1)\cdot\left(1 - GT\cdot\left(SoC_{t_0}, 1\right)\right) - EQL(SIGNAL\_EXT, -1)\cdot\left(1 - LT\left(SoC_{t_0}, 0\right)\right) \quad (1)$$

where *SIGNAL_EXT* is the parameter representing the signal for discharging or charging according to external conditions, like energy demand, weather conditions, energy prices, etc; SoC_{t_0} is the state of charge of the TCM at the previous time t_0. Equations were defined using the following TRNSYS mathematical functions:

- $EQL(\cdots, \cdots)$ returns 1 if first expression is equal to second; returns 0 otherwise;
- $GT(\cdots, \cdots)$ returns 1 if first expression in parentheses is greater than second; returns 0 otherwise;
- $LT(\cdots, \cdots)$ returns 1 if first expression in parentheses is lower than second; returns 0 otherwise.

The state of charge of the TCM at the time t was evaluated using Eq. (2):

$$SoC(t) = SoC_{t_0} - \Delta SoC\cdot EQL(SIGNAL, -1) + \Delta SoC\cdot EQL(SIGNAL, 1) \quad (2)$$

where ΔSoC is the difference in state of charge between the previous time t_0 and the time t, and it was calculated as:

$$\Delta SoC = dm_{w_t}/m_{w_{max}} \quad (3)$$

where dm_{w_t} is the water mass adsorbed or desorbed [g] in the timestep Δt, equal to $t - t_0$ [h]; $m_{w_{max}}$ is the maximum mass adsorbed or desorbed [g] in the period t_{max} [h], as reported in Table 2. The period t_{max} was assessed as:

$$t_{max} = m_{w_{max}}/\dot{R}_{max} \quad (4)$$

where $\dot{R}_{max}$ is the maximum adsorption or desorption rate [g/h], obtained by multiplying the maximum specific adsorption or desorption rate $\dot{r}_{max}$ and the TCM mass. Therefore, stopping criteria are represented by the TCM state of charge *SoC* (more precisely by the state of charge of the TCM at the previous time t_0, SoC_{t_0}) and by the *SIGNAL_EXT* parameter. The energy released or stored at the time t was evaluated using Eq. (5):

$$E(t) = min\Big(E_{t_0} + \dot{Q}_t\cdot\Delta t\cdot EQL(SIGNAL, -1) - \dot{Q}_t\cdot\Delta t\cdot EQL(SIGNAL, 1); E_{max}\Big) \quad (5)$$

where E_{t_0} is the energy released or stored at the previous time t_0 [Wh]; $\dot{Q}_t$ is the thermal power released or stored at the time t [W]; E_{max} is the maximum energy that can be released or stored in the period t_{max} [Wh].

Here, $\dot{Q}_t$ was calculated as:

$$\dot{Q}_t = \dot{Q}_{max}\cdot pm \quad (6)$$

where $\dot{Q}_{max}$ is the maximum power releasable or storable [W], obtained by multiplying the specific thermal power $\dot{q}_{max}$ and the TCM mass; pm is the power modulation parameter evaluated according to the building heating thermal load:

$$pm = \dot{Q}_{load_t}/\dot{Q}_{load_{max}} \quad (7)$$

where $\dot{Q}_{load_t}$ is the building heating load at the time t [W], and $\dot{Q}_{load_{max}}$ is

the peak heating load [W].

Similarly, $m_w(t)$ the mass of water adsorbed or desorbed [g] at the time t was evaluated as:

$$m_w(t) = \min\left(m_{w_{t_0}} + \dot{R}_t \cdot \Delta t; m_{w_{max}}\right) \quad (8)$$

where $m_{w_{t_0}}$ is the mass adsorbed [g] at the previous time t_0, $\dot{R}_t$ is the water adsorption or desorption rate at the time t [g/h], calculated as:

$$\dot{R}_t = \dot{R}_{max} \cdot pm \quad (9)$$

Therefore, the main control parameter is the power modulation parameter pm, used to define both the thermal power released or stored at the time t, $\dot{Q}_t$, according to Eq. (6), and to calculate the water adsorption or desorption rate at the time t, $\dot{R}_t$, using Eq. (9). The hourly heating load profile, defined by TRNSYS over a year, of a common 80 m^2 domestic building located in Ferrara was assumed to define the pm parameter. Outdoor environmental conditions (like outdoor air temperatures, solar radiation, etc.) for the year 2023 were acquired by the weather station [49] installed outside the mock-up in Ferrara, and considered to create the weather data file used by TRNSYS. Thermal properties of the building and main boundary conditions used in simulations to define the heating load profile are summarised in Table 3.

As regards the psychrometric conditions of inlet and outlet airflow, the difference in enthalpy ΔJ [kJ/kg] and humidity ratio ΔX [g/kg] was calculated according to $\dot{Q}_t$ and $m_w(t)$, using Eq. (10) and Eq. (11), respectively:

$$\Delta J = \left(\dot{Q}_t \Big/ \dot{m}_{air}\right) \cdot 3.6 \quad (10)$$

$$\Delta X = \dot{R}_t / \dot{m}_{air} \quad (11)$$

where $\dot{m}_{air}$ is the mass flow rate of air [kg/h].

The equations defining $E(t)$, $m_w(t)$ and $SoC(t)$ as reported above allowed to simulate a realistic operation of the reactor, alternating discharging and charging with standby periods. When the system stopped at a defined time, it was possible to evaluate the current SoC, the available remaining energy $E_{max} - E(t)$ and the remaining water to be adsorbed or desorbed $m_{w_{max}} - m_w(t)$, before a new turning on, thus supporting the definition of the control system. For the sake of brevity, the operation of the reactor solely during the discharging process is described in the following lines. The behaviour of the TCM reactor starting from a standby mode at the time = 0 h, with a SoC slightly lower than 72 %, an initial energy E equal to nearly 10 Wh and an initial water mass m_w equal to about 20 g is illustrated in Fig. 5. The contemporary conditions at the time t_0 of $SIGNAL\_EXT$ = -1, due to the building heating demand, and of SoC higher than 0 resulted in a $SIGNAL = -1$, which made the reactor operate in discharging mode for the timestep Δt, equal to $t - t_0$. At the time t, with a SoC decreased up to 32 %, a remaining energy E of 10 Wh and a remaining water mass m_w to be adsorbed equal to almost 27 g, the reactor stopped due to the negligible heating demand. Then, the heating demand made the reactor operate in discharging mode again, until the system reached a $SoC = 0$, the E_{max} was released, and the water mass was completely adsorbed.

Table 3
Properties of the building envelope and boundary conditions used in simulations.

Component	Surface [m^2]	Thermal transmittance[W/(m^2·K)]
Window	42	1.10
External wall	157	0.28
Ground Floor	80	0.30
Roof	80	0.13
Boundary condition	**Value**	**m.u.**
Infiltrations	0.10	[1/h]
Internal loads	110	[W]
Heating setpoint temperature	20	[°C]

2.3. Preliminary validation of the model

The TRNSYS model of the ECHO system was preliminarily validated by using the design values of the plant prototype to be installed in Ferrara, awaiting the more accurate and reliable validation that will be conducted on the base of the monitoring data that will be collected. Design values of the system used for the preliminary validation of the model are reported in Table 4.

The comparison between design values of air temperature and humidity ratio and simulation results obtained by using the design parameters reported in Table 3 showed a good reliability of the model, as illustrated in Fig. 6. Considered that enthalpy is the most significant parameter, percentage deviations between design and simulated enthalpy values for each condition have been reported in Fig. 6.

3. Dynamic simulations

Firstly, a series of simulations were conducted to ideally investigate the capacity of TCM to solely meet the building heating demand. Four TCM mass quantities were considered: 100, 120, 140 and 160 kg. Charging was allowed when the building thermal load at the time t $\dot{Q}_{load_t}$ was lower than 30 % of the peak heating load $\dot{Q}_{load_{max}}$, that is, when power modulation pm was lower than 0.3. Then, the optimal quantity was assumed to investigate two additional charging control strategies (CHS). To summarise, three various conditions for setting $SIGNAL\_EXT = 1$, i.e. allowing charging, were analysed:

- CHS0: when pm<0.3;
- CHS1: when pm<0.3, during the time 10:00–16:00;
- CHS2: when pm<0.3 and solar radiation is higher than 300 W/m^2.

The scenarios CHS1 and CHS2 were aimed at considering the potential contribution of renewable energy coming from PV/T panels, when available, to cover the energy needed for charging TCM.

The results achieved highlighted the critical risks of relying exclusively on TCM to meet the building heating load, but they also uncovered its valuable contribution if integrated with an auxiliary system like a heat pump. Thus, a comparative analysis between the performance of the ECHO system (identified as HP-TCM system) and of the system without TCM (identified as HP system) was carried out. The ultimate objective of the study was to investigate how much TCM is able to increase the efficiency of the system where it is integrated. In the ECHO system, the thermal contribution of TCM was provided to the user water storage tank through the cooling coil. Here, hot air flowing out of the TCM reactor, after having been heated and dehumidified during the discharging process, exchanged the heat generated with the hydronic loop (phase 1-2 in Fig. 1 and Fig. 2) to be then stored in the user tank and finally employed to meet the building heating demand. Differently, in the system without TCM, thermal contribution to the user tank was provided exclusively by the heat pump. Therefore, the thermal contribution E_{th} to the user tank and the electrical energy consumption E_{el} of the two systems were analysed over the heating season, and their monthly and seasonal COP were compared. The main assumptions, control strategies, and operating conditions used in simulations are reported in the following lines.

Type 534 was used to simulate the 300 L user tank, that was equipped with 3 ports in the HP-TCM system. One inlet/outlet port was connected to the heat pump, with a water mass flow rate of 1440 kg/h, a second port was destined for the cooling coil, with a water mass flow rate of 720 kg/h, and the third one was connected to the user side to provide space heating. Type 927 was used to simulate the water-to-

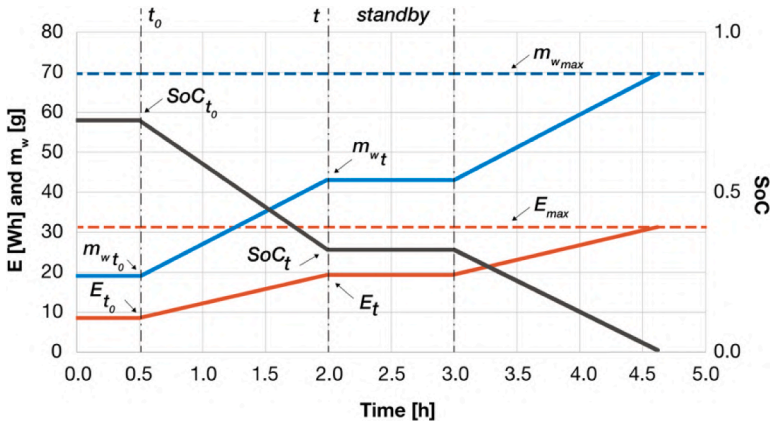

Fig. 5. Thermal performance of the TCM reactor, discharging phase.

water heat pump ($\dot{Q}_{heating}$ of 8 kW, user 40/45 °C – source 0/-3 °C). Control of the heat pump operation was carried out via a differential controller with hysteresis (Type 2b), where setpoint temperature of the outlet water on the user side was set equal to 45 °C with an upper and lower dead band temperature of 5 °C and 0 °C, respectively. Thereby, the heat pump was turned on whenever the user tank on the user side needed to be recharged to the seasonal target temperature. On the source side, the heat pump was assumed to be connected to horizontal ground heat exchangers. A comprehensive description of the type of horizontal ground heat exchangers technology and results achieved in an experimental large-scale installation are reported in [50]. Type 508 was employed to simulate the cooling coil, which operated when the TCM reactor was in discharging mode. Differently, the user tank was equipped with 2 ports in the HP system configuration, one for the heat pump and the other one for the user side.

Whilst the thermal contribution $E_{th_{HP}}$ supplied by the heat pump and the related electrical energy consumption $E_{el_{HP}}$ were directly extracted from simulation results as outputs of the type 927 used for the heat pump, the thermal contribution $E_{th_{CC}}$ provided by the cooling coil to the tank was calculated according to Eq. (12):

$$E_{th_{CC}} = \dot{m}_{CC} \cdot c_p \cdot \Delta T_{CC} \cdot t_{dis} \quad (12)$$

where $\dot{m}_{CC}$ is the outlet mass flow rate of water from the cooling coil into the tank [kg/h], c_p is water specific heat equal to 4.186 [kJ/(kg·K)], ΔT_{CC} is the temperature difference between outlet and inlet water from the cooling coil, and t_{dis} is the time [h] of operation in discharging mode. As for the evaluation of the electrical energy consumption connected to the cooling coil $E_{el_{CC}}$, this was considered to be equal to the sole electrical energy consumption E_{el} of the reactor fan during discharging mode. Indeed, the charging process of TCM was assumed to be ideally carried out by using renewable energy coming from PV/T or other renewable energy sources. Therefore, $E_{el_{CC}}$ was evaluated as:

$$E_{el_{CC}} = \dot{Q}_{fan} \cdot t_{dis} \quad (13)$$

where $\dot{Q}_{fan}$ is the fan power, equal to 120 W, and t_{dis} is the time [h] of operation of the fan during discharging.

Simulations were carried out over the heating period, from October to March 2023, with a timestep of 5 min. CHS1 was assumed.

Finally, the thermal contribution of the two combined TES systems, TCM and PCM, was examined. PCM integrated in the water storage tank was employed to preheat the airflow at the inlet of the heat recovery unit. Latent heat released during PCM solidification was transferred to air during the discharging mode by means of an air-to-water heat exchanger (phase 7-8 in Fig. 2). The non-standard Type 840 was used to simulate the 200 L PCM integrated storage tank, which was coupled to Type 753 for the air-to-water heat exchanger.

The thermal power $\dot{Q}_{th_{TCM}}$ provided by the cooling coil to the user tank was calculated according to Eq. (14):

$$\dot{Q}_{th_{TCM}} = \dot{m}_{CC} \cdot c_p \cdot \Delta T_{CC} \quad (14)$$

where $\dot{m}_{CC}$ is the outlet mass flow rate of water from the cooling coil into the tank [kg/h], c_p is water specific heat equal to 4.186 [kJ/(kg·K)], ΔT is the temperature difference between outlet and inlet water from the cooling coil. The thermal power $\dot{Q}_{th_{PCM}}$ provided by the PCM was evaluated according to Eq. (15):

$$\dot{Q}_{th_{PCM}} = \dot{m}_{PCM} \cdot c_p \cdot \Delta T_{PCM} \quad (15)$$

where $\dot{m}_{PCM}$ is the outlet mass flow rate of water from the PCM integrated tank [kg/h], c_p is water specific heat equal to 4.186 [kJ/(kg·K)], ΔT is the temperature difference between outlet and inlet water from the tank. Furthermore, the total thermal energy provided by the two TES systems, $E_{th_{TCM}}$ and $E_{th_{PCM}}$, was evaluated and compared to the building heating demand. A 1-week period characterised by the highest values of heating demand was considered, from January 16th to 22nd.

4. Results and discussion

4.1. TCM quantities and CHSs

Simulation results comparing the ability of different TCM quantities to meet the building heating demand throughout the year, without the support of any auxiliary device, are presented in the following lines. Average values of the ratio between the hourly thermal power generated by the TCM $\dot{Q}_t$ and the hourly building heating demand $\dot{Q}_{load_t}$ are reported in Table 5, while the hourly trend for the four TCM quantities over the year is illustrated in Fig. 7. Results in Table 5 showed that only the scenarios with 140 and 160 kg of TCM ensured an average ratio close to 1. Considered that the power modulation parameter *pm* (equal to the ratio between the building heating load at the time *t* $\dot{Q}_{load_t}$ and the peak heating load $\dot{Q}_{load_{max}}$) was higher than 0 for 3901 h, the number of h when the $\dot{Q}_t$ produced by the TCM was higher than the building heating demand $\dot{Q}_{load_t}$ ranged from 58 h for 100 kg of TCM up to 3667 and 3831 h for 140 and 160 kg of TCM. Similarly, taking into account the number of hours when $\dot{Q}_t$ was higher than 90 % of $\dot{Q}_{load_t}$, 3425 h were ensured with 120 kg of TCM, while values higher than 3800 were achieved with 140 and 160 kg. As for the ratio between the number of h when $\dot{Q}_t > \dot{Q}_{load_t}$ (or $\dot{Q}_t > 90\ \% \dot{Q}_{load_t}$) and the h when $pm > 0$, values higher than 90 % where obtained only with 140 and 160 kg of TCM.

Results of the analysis of the three control strategies for triggering charging signal are reported below. The three strategies were compared in terms of *SoC* reached over the first three months of the year 2023

Table 4
Design values of the system used for the preliminary validation of the model.

Phase	Parameter	Discharging	Charging	Unit
–	$\dot{m}_{air}$	950	720	[kg/h]
1–2	T_{in}	50.0	80.0	[°C]
	X_{in}	20.0	8.0	[g/kg]
	T_{out}	75.7	51.3	[°C]
	X_{out}	12.7	16.6	[g/kg]
2–3	T_{in}	75.7	–	[°C]
	X_{in}	12.7	–	[g/kg]
	T_{out}	67.6	–	[°C]
	X_{out}	12.7	–	[g/kg]
	T_{win}	50.0	–	[°C]
	T_{wout}	55.0	–	[°C]
3–4	T_{in}	75.7	–	[°C]
	X_{in}	12.7	–	[g/kg]
	T_{out}	67.6	–	[°C]
	X_{out}	12.7	–	[g/kg]
4–5	η	84.5	84.5	[%]
	T_{in}	67.6	51.3	[°C]
	X_{in}	12.7	16.6	[g/kg]
	T_{out}	43.0	24.2	[°C]
	X_{out}	12.7	14.7	[g/kg]
5–6	$\dot{m}_{whum}$	36.0	–	[kg/h]
	T_{in}	43.0	–	[°C]
	X_{in}	12.7	–	[g/kg]
	T_{out}	25.0	–	[°C]
	X_{out}	20.0	–	[g/kg]
6–7	T_{in}	–	24.2	[°C]
	X_{in}	–	14.7	[g/kg]
	T_{out}	–	11.3	[°C]
	X_{out}	–	8.0	[g/kg]
	T_{win}	–	7.5	[°C]
	T_{wout}	–	12.5	[°C]
	$\dot{m}_{wevap}$	–	1150	[kg/h]
7–8	T_{in}	25.0	–	[°C]
	X_{in}	20.0	–	[g/kg]
	T_{out}	27.6	–	[°C]
	X_{out}	20.0	–	[g/kg]
	T_{win}	35.0	–	[°C]
	T_{wout}	30.0	–	[°C]
	$\dot{m}_{wPCM}$	430	–	[kg/h]
8–9	η	84.5	84.5	[%]
	T_{in}	27.6	11.3	[°C]
	X_{in}	20.0	8.0	[g/kg]
	T_{out}	50.0	44.6	[°C]
	X_{out}	20.0	8.0	[g/kg]
9–10	T_{in}	–	44.6	[°C]
	X_{in}	–	8.0	[g/kg]
	T_{out}	–	80.0	[°C]
	X_{out}	–	8.0	[g/kg]
	T_{win}	–	82.0	[°C]
	T_{wout}	–	77.0	[°C]
	$\dot{m}_{wcond}$	–	1230	[kg/h]
10–11	$\dot{q}$	–	2	[kW]
	T_{in}	–	80.0	[°C]
	X_{in}	–	8.0	[g/kg]
	T_{out}	–	90.0	[°C]
	X_{out}	–	8.0	[g/kg]

(Fig. 8) and in terms of hours of operation in discharging mode over a 1-week period in January (Fig. 9). The possibility to recharge TCM whenever the building heating load $\dot{Q}_{load_t}$ was lower than 30 % of the peak heating load $\dot{Q}_{load_{max}}$, according to CHS0, allowed to reach either higher or lower values of *SoC*, up to 0.39 and -0.13, with an average *SoC* of 0.01, as illustrated in Fig. 8. Differently, the CHS1 brought to a mean *SoC* of 0.01, with maximum and minimum values equal to 0.08 and -0.04, respectively. Consequently, the even more limiting CHS2 resulted in an average *SoC* of -0.02, which reached 0.08 and -0.1 as the highest and lowest values. The quantity of hours during which the system operated in discharging mode to comply with the discharging *SIGNAL_EXT* over a 1-week in January are illustrated in Fig. 9. Results showed that CHS0 allowed to operate discharging 98 % of the time it was requested by the *SIGNAL_EXT*. Conversely, CHS1 made the system operate in discharging mode 32 % of the time against what it was needed, whilst with CHS2 the discharging time decreased up to 9 %.

4.2. Performance of the ECHO system and of the system without TCM

A comparative analysis between the performance of the system without the TCM contribution (identified as HP system) (Table 6) and the ECHO system (identified as HP-TCM system) (Table 7) was conducted. More in detail, the thermal contribution E_{th} provided by the heat pump and by the cooling coil to the user tank, and the electrical energy consumption E_{el} related to the heat pump and to the cooling coil, were analysed over the heating season, and their monthly and seasonal COP were evaluated.

The percentage variation in the electrical energy consumption of the HP-TCM system compared to the HP system is reported in Table 7, where it is identified as $\Delta E_{el(HP-TCM\ VS\ HP)}$. Results highlighted that TCM contribution in the HP-TCM system allowed to reduce the seasonal electricity consumption related to the HP and to the cooling coil ($E_{el_{HP-TCM}}$) by about 8.8 % compared to the heat pump system without TCM ($E_{el_{HP}}$), and by nearly 8.4 % if data regarding October are not included in the analysis. Indeed, as reported by the data collected through the weather station [49] installed in Ferrara and considered to generate the weather data file used in simulations, outdoor air temperatures in October have been particularly higher in the last years (average outdoor air temperature in 2023 was equal to 19.8 °C, with a minimum and maximum of 14.5 °C and 26.6 °C, respectively), resulting in extremely low heating demand. According to the same heating period, energy savings on electrical energy consumption $\Delta E_{el_{HP-TCM}}$ range from 6.2 % in January up to 13.7 % in March.

The valuable cut in electrical energy use brought to a significant increase in the equivalent COP of the HP-TCM system compared to the system without TCM. The seasonal COP_{HP-TCM} was equal to 3.8, whilst COP_{HP} was 3.4, as reported in Table 7 and in Table 6, respectively. Furthermore, if a reduced heating period, starting from November, is considered as mentioned above, a seasonal COP_{HP-TCM} of 3.7 was evaluated, with monthly values varying from 3.4 in January to 4.7 in November. For a comprehensive interpretation of the results, it should be noted that the thermal contribution provided to the tank is characterised by slight differences between the HP system ($E_{th_{HP}}$ in Table 6) and the HP-TCM system ($E_{th_{HP-TCM}}$ in Table 7). Nevertheless, seasonal discrepancy is equal to almost 0.5 %, with monthly values ranging from 0.8 % to 0.4 %. The difference, although quite modest, is due to the fact that in the context of the dynamic simulations conducted the user tank cannot be ideally simulated as a unique thermal node, thus as a unique storage unit. However, as mentioned above, variations are extremely slight (< 1 %) and neglectable.

4.3. Thermal contribution of TCM integrated with PCM

The thermal contribution of the two combined TES systems, TCM and PCM, over a 1-week period is illustrated in Fig. 10a. The week characterised by the highest values of heating demand, i.e. from January 16th to 22nd, was selected. Temperature differences generated by the PCM and the TCM are also reported (Fig. 10b).

Results highlighted an average thermal power from the PCM $\dot{Q}_{th_{PCM}}$ of 0.7 kW and an average thermal power from the cooling coil $\dot{Q}_{th_{TCM}}$ equal to nearly 1.5 kW, with mean values of temperature difference equal to 1.9 °C and 2.6 °C for PCM and TCM, respectively. The daily thermal energy extracted from the two TES systems compared to the heating energy demand is reported in Table 8. Thermal energy provided by PCM was ranging from 1.4 % to 5.0 %, with an average value of nearly 3 %, while thermal energy extracted from TCM was varying from 3.3 % up to 10.6 %, with an average value of about 6 %. Thus, the two TES systems were able to cover about 10 % of the heating energy demand, with the PCM providing almost 50 % of the TCM contribution.

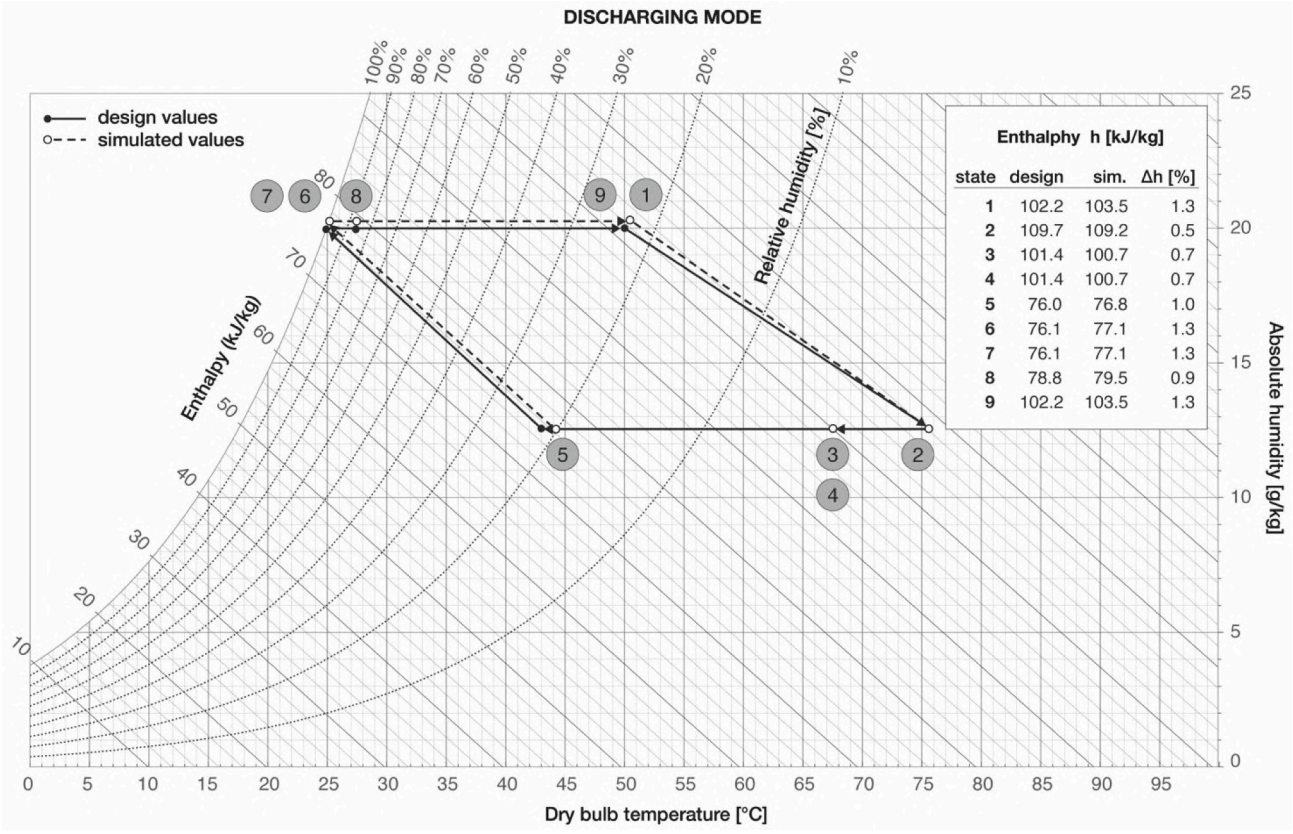

Fig. 6. Psychrometric conditions during discharging: design values and simulated values.

Table 5
Performance of different TCM quantities in meeting the building heating demand.

	100	120	140	160	[kg_{TCM}]
$\dot{Q}_t/\bar{\dot{Q}}_{load_t}$	0.70	0.84	0.98	1.12	[W/W]
$\dot{Q}_t > \dot{Q}_{load_t}$	58	300	3667	3831	[H]
$\dot{Q}_t > 90\%\dot{Q}_{load_t}$	130	3425	3806	3876	[H]
$pm > 0$	3901	3901	3901	3901	[H]
$(\frac{\dot{Q}_t > \dot{Q}_{load_t}}{pm > 0})$	0.01	0.08	0.94	0.98	[h/h]
$(\frac{\dot{Q}_t > 90\%\dot{Q}_{load_t}}{pm > 0})$	0.03	0.88	0.98	0.99	[h/h]

5. Conclusions

A novel TCM integrated system was numerically modelled in TRNSYS, the control algorithm was developed and implemented, and preliminary results illustrating the operation of the control algorithm were presented. The model reproduced a closed-loop reactor that combines TCMs with PCMs, which was simulated in dynamic mode and at system scale, i.e. including both the TCM reactor and auxiliary devices.

The ideal analysis of the optimal TCM mass able to solely cover the building heating demand highlighted that the ratio between the number of hours when $\dot{Q}_t > \dot{Q}_{load_t}$ and the hours when $\dot{Q}_{load_t}/\dot{Q}_{load_{max}} > 0$ was equal to 94 % and 98 % with 140 and 160 kg of TCM, whilst was lower than 10 % with 120 kg (where $\dot{Q}_t$ is the thermal power released or stored by TCM at the time t; $\dot{Q}_{load_t}$ is the building heating load at the time t;

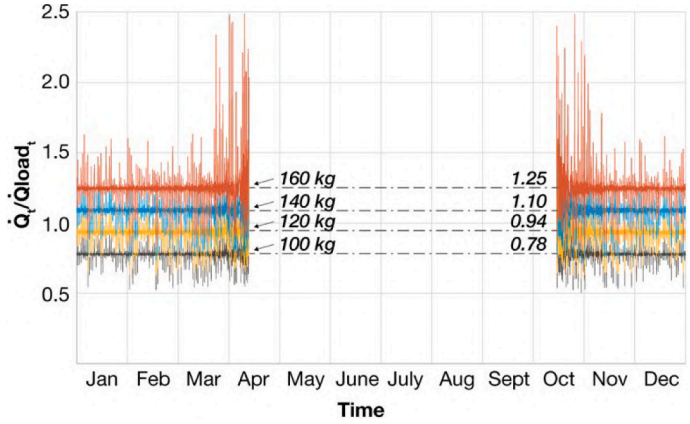

Fig. 7. Ratio between the $\dot{Q}_t$ produced by 100, 120, 140 and 160 kg of TCM and the building $\dot{Q}_{load_t}$.

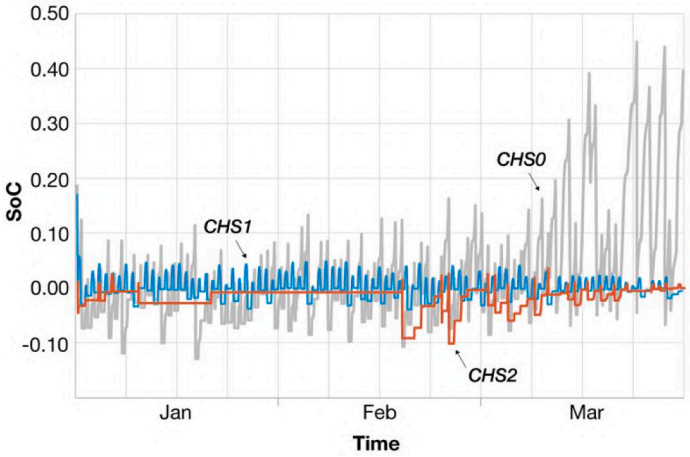

Fig. 8. SoC achieved with CHS0, CHS1 and CHS2 during January, February and March 2023.

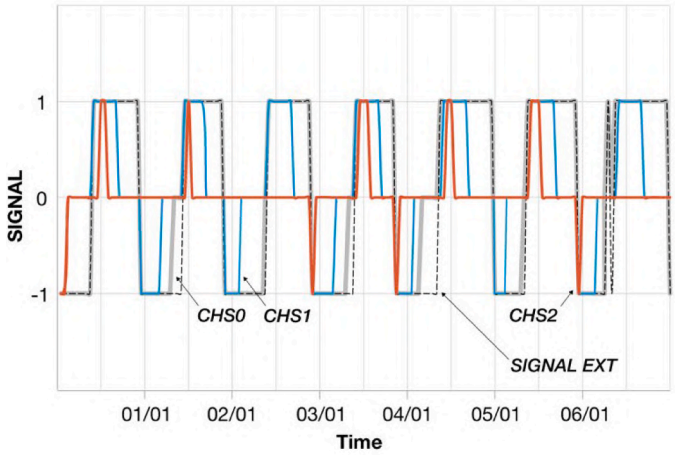

Fig. 9. Operating modes set with CHS0, CHS1 and CHS2 in relation to the curve of SIGNAL_EXT during a 1-week in January 2023.

Table 6
Monthly and seasonal E_{th} provided by the heat pump, related E_{el} and COP of the HP system.

	HP		
	$E_{th_{HP}}$ [kWh]	$E_{el_{HP}}$ [kWh]	COP_{HP} [–]
Jan	2,691	841	3.2
Feb	2,053	638	3.2
March	1,267	363	3.5
Oct	240	50	4.8
Nov	1,438	352	4.1
Dec	2,415	711	3.4
Total	**10,104**	**2,955**	**3.4**

$\dot{Q}_{load_{max}}$ is the peak heating load). Findings suggested that there is a non-linear correlation between the amount of TCM used and the heating demand covered. However, the existence of a critical threshold under which TCM efficiency drastically reduces may be due to the extremely basic and rough control strategy. Thus, the adoption of accurate control strategies is crucial to optimise the amount of TCM.

Simulation results about the three charging control strategies showed that CHS0 (which enabled charging when $pm < 0.3$, where pm is the ratio between $\dot{Q}_{load,}$ and $\dot{Q}_{load_{max}}$) allowed the system to operate in discharging mode 98 % of the time it was requested, reaching an average and maximum value of SoC equal to 0.01 and 0.39, respectively. Nevertheless, the high availability of TCM in covering heating demand whenever it was required could significantly impact on the electrical energy needed to carry out TCM charging, especially considered the intermittent nature of renewable energy sources. Differently, CHS1 (allowing charging when $pm < 0.3$, between 10:00 and 16:00) resulted in operate discharging for 32 % of the time against what it was required, with a mean and maximum SoC of 0.01 and 0.08, respectively. Even lowest values were obtained with CHS2 (enabling charging when $pm <$ 0.3 and solar radiation was higher than 300 W/m^2). However, despite the significantly lower TCM availability compared to the one obtained with CHS0, the adoption of CHS1 may result far more efficient in optimising the use of TCM, as it fosters the exploitation of renewable energy sources like solar energy for the charging process.

Findings reported above highlighted the critical risks of relying exclusively on TCM to meet the building heating load, but also uncovered its valuable contribution if integrated with an auxiliary system like a heat pump (HP) in the ECHO system. The comparative analysis of the performance of the HP-TCM system and of the HP system highlighted that the former allowed to achieve an 8.8 % reduction in seasonal electricity consumption, and an increase in the seasonal COP from 3.4 to 3.8. Finally, the daily thermal contribution provided by the two TES systems, TCM combined with PCM, compared to the building heating demand was evaluated over a 1-week period in January. Research results showed that the two TES systems were able to cover about 10 % of the heating energy demand, with PCM providing almost 50 % of the TCM contribution.

Table 7
Monthly and seasonal E_{th} provided by the heat pump and by the cooling coil, related E_{el} and COP of the HP-TCM system.

	HP		CC			HP-TCM			
	$E_{th_{HP}}$ [kWh]	$E_{el_{HP}}$ [kWh]	$E_{th_{CC}}$ [kWh]	$E_{th_{CC}}/E_{th_{HP-TCM}}$ [%]	$E_{el_{CC}}$ [kWh]	$E_{th_{HP-TCM}}$ [kWh]	$E_{el_{HP-TCM}}$ [kWh]	$\Delta E_{el}(HP-TCM\ VS\ HP)$ [%]	COP_{HP-TCM} [–]
Jan	2,549	783	153	5.7	6	2,702	789	−6.2	3.4
Feb	1,930	587	133	6.5	5	2,063	592	−7.1	3.5
March	1,133	309	144	11.3	5	1,277	314	−13.7	4.1
Oct	198	33	46	18.8	0	243	33	−34.7	7.5
Nov	1,320	304	127	8.8	5	1,447	309	−12.4	4.7
Dec	2,276	654	151	6.2	5	2,426	659	−7.3	3.7
Total	9,404	2,669	754	7.4	26	10,158	2,695	−8.8	3.8

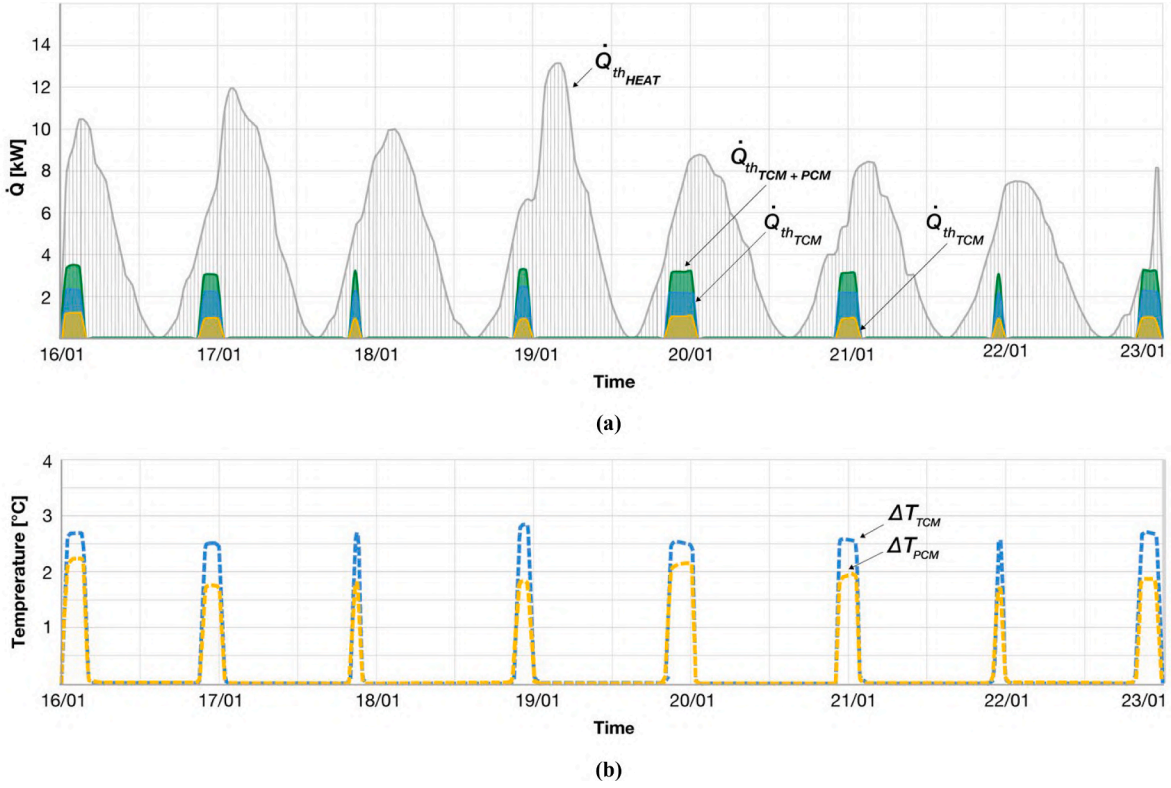

Fig. 10. Thermal contribution (a) and temperature differences (b) generated by TCM and PCM over 1-week in January 2023.

Table 8
Daily thermal energy provided by PCM ($E_{th\,PCM}$) and TCM ($E_{th\,TCM}$) compared to the heating energy demand ($E_{th\,HEAT}$) over 1-week in January 2023.

		16/01	17/01	18/01	19/01	20/01	21/01	22/01
$E_{th\,PCM}$	[kWh]	5.1	1.8	1.7	3.1	2.0	2.8	2.8
$E_{th\,TCM}$	[kWh]	10.9	4.3	4.7	6.3	4.2	6.4	6.7
$E_{th\,PCM+TCM}$	[kWh]	16.0	6.2	6.4	9.4	6.2	9.2	9.5
$E_{th\,HEAT}$	[kWh]	102.5	130.0	107.9	131.6	92.1	90.6	80.8
		16/01	**17/01**	**18/01**	**19/01**	**20/01**	**21/01**	**22/01**
$E_{th\,PCM}/E_{th\,HEAT}$	[%]	5.0	1.4	1.6	2.4	2.1	3.1	3.5
$E_{th\,TCM}/E_{th\,HEAT}$	[%]	10.6	3.3	4.3	4.8	4.6	7.1	8.3
$E_{th\,PCM+TCM}/E_{th\,HEAT}$	[%]	15.6	4.7	6.0	7.1	6.7	10.2	11.8

The findings reported above emphasise the limitations of relying exclusively on TCM to meet the building heating demand. Indeed, despite its valuable potential, TCM efficiency is significantly enhanced when integrated with auxiliary systems, such as a heat pump, as seen in the ECHO system. Within this framework, control strategies should thoroughly consider the opportunity to operate in discharging mode, and use TCM to partially meet the building energy demand, and the need to recharge TCM by exploiting renewable energy sources like solar energy. Otherwise, the use of TCM results to be not advantageous. Additionally, the research results uncovered a non-linear relationship between the amount of TCM and the heating demand covered. This highlights the importance of implementing accurate and refined control strategies to optimise TCM mass.

However, for the sake of completeness, it should be noted that the effectiveness of TCM systems does not only depend on the share of renewable energy used for the charging process. Rather, their

performance is also ensured by the availability of surplus electricity from the grid, the potential for harnessing waste heat, etc. Furthermore, TCM efficiency is determined by the careful selection of materials, the system design, and operational efficiencies. For these reasons, considering the future scope of the study, the work is progressing with the definition of control strategies aimed at the exploitation of renewable energy sources for TCM charging, as well as at the exploration of virtuous synergies when considering the system integrated in the network. In addition, different TCM materials, impregnation methods, particle size and operating conditions are currently under investigation and are being tested.

Among the limitations of the present study there is the fact that the results and observations reported above are derived from a numerical model and not from experimental data collected from a prototype. Thus, as a future development of the work, the TRNSYS model of ECHO system will be calibrated with the monitoring data of the prototype that will be installed in Ferrara, and used to refine the preliminary control rules and the control system to be implemented in the three real test cases.

Declaration of competing interest

The authors declare that they have no known competing financial interests or personal relationships that could have appeared to influence the work reported in this paper.

Acknowledgements

This work was supported financially within the ECHO project – Efficient Compact modular tHermal energy stOrage system – funded by the European Union's Horizon Europe research and innovation programme under grant agreement No. 101096368.

Data availability

The data that has been used is confidential.

References

[1] European Council. European Green Deal. https://www.consilium.europa.eu/en/policies/green-deal/, 2023 [Accessed 23 July 2024].
[2] L.F. Cabeza, Advances in thermal energy storage systems: methods and applications, in: L.F. Cabeza (Ed.), Advances in Thermal Energy Storage Systems (second ed.), Woodhead Publishing, Cambridge, 2021, pp. 37–54, https://doi.org/10.1016/B978-0-12-819885-8.00002-4.
[3] E. Borri, G. Zsembinszki, L.F. Cabeza, Recent developments of thermal energy storage applications in the built environment: a bibliometric analysis and systematic review, Appl. Therm. Eng. 189 (2021) 116666, https://doi.org/10.1016/j.applthermaleng.2021.116666.
[4] H. Bao, Z. Ma, Thermochemical energy storage, in: T.M. Letcher (Ed.), Storing Energy (second edition), Elsevier, Amsterdam, 2022, pp. 651–683.
[5] G. Krese, R. Koželj, V. Butala, U. Stritih, Thermochemical seasonal solar energy storage for heating and cooling of buildings, Energy Build. 164 (2018) 239–253, https://doi.org/10.1016/j.enbuild.2017.12.057.
[6] Z. Ma, H. Bao, A.P. Roskilly, Electricity-assisted thermochemical sorption system for seasonal solar energy storage, Energy Convers. Manage. 209 (2020) 112659, https://doi.org/10.1016/j.enconman.2020.112659.
[7] G. Manente, Y. Ding, A. Sciacovelli, A structured procedure for the selection of thermal energy storage options for utilization and conversion of industrial waste heat, J. Energy Storage 51 (2022) 104411, https://doi.org/10.1016/j.est.2022.104411.
[8] K. Kant, R. Pitchumani, Advances and opportunities in thermochemical heat storage systems for buildings applications, Appl. Energy 321 (2022) 119299, https://doi.org/10.1016/j.apenergy.2022.119299.
[9] K. Moulakhnif, H.A. Ousaleh, S. Sair, Y. Bouhaj, A. El Majd, M. Ghazoui, A. Faik, A. El Bouari, Renewable approaches to building heat: exploring cutting-edge innovations in thermochemical energy storage for building heating, Energy Build. 318 (2024) 114421, https://doi.org/10.1016/j.enbuild.2024.114421.
[10] O. Kazaz, N. Karimi, M.C. Paul, Optically functional bio-based phase change material nanocapsules for highly efficient conversion of sunlight to heat and thermal storage, Energy 305 (2024) 132290, https://doi.org/10.1016/j.energy.2024.132290.
[11] O. Kazaz, N. Karimi, S. Kumar, G. Falcone, M.C. Paul, Thermally enhanced nanocomposite phase change material slurry for solar-thermal energy storage, J. Energy Storage 78 (2024) 110110, https://doi.org/10.1016/j.est.2023.110110.
[12] O. Kazaz, N. Karimi, S. Kumar, G. Falcone, M.C. Paul, Heat transfer characteristics of fluids containing paraffin core-metallic shell nanoencapsulated phase change materials for advanced thermal energy conversion and storage applications, J. Mol. Liq. 385 (2023) 122385, https://doi.org/10.1016/j.molliq.2023.122385.
[13] R.A. Lawag, H.M. Ali, Phase change materials for thermal management and energy storage: a review, J. Energy Storage 55 C 105602 (2022), https://doi.org/10.1016/j.est.2022.105602.
[14] A.T. Muzhanje, M.A. Hassan, H. Hassan, Phase change material based thermal energy storage applications for air conditioning: review, Appl. Therm. Eng. 214 (2022) 118832, https://doi.org/10.1016/j.applthermaleng.2022.118832.
[15] S. Cesari, E. Baccega, G. Emmi, M. Bottarelli, Enhancement of a radiant floor with a checkerboard pattern of two PCMs for heating and cooling: results of a real-scale monitoring campaign, Appl. Therm. Eng. 246 (2024) 122887, https://doi.org/10.1016/j.applthermaleng.2024.122887.
[16] Y. Xu, B.B. Sun, L.J. Liu, X.Y. Liu, The numerical simulation of radiant floor cooling and heating system with double phase change energy storage and the thermal performance, J. Energy Storage 40 (2021) 102635, https://doi.org/10.1016/j.est.2021.102635.
[17] S. Cesari, G. Emmi, M. Bottarelli, A weather forecast-based control for the improvement of PCM enhanced radiant floors, Appl. Therm. Eng. 206 (2022) 118119, https://doi.org/10.1016/j.applthermaleng.2022.118119.
[18] Y. Xia, X.S. Zhang, Experimental research on a double-layer radiant floor system with phase change material under heating mode, Appl. Therm. Eng. 96 (2016) 600–606, https://doi.org/10.1016/j.applthermaleng.2015.11.133.
[19] M. Saffari, C. Roe, D.P. Finn, Improving the building energy flexibility using PCM-enhanced envelopes, Appl. Therm. Eng. 25 (2022) 119092, https://doi.org/10.1016/j.applthermaleng.2022.119092.
[20] R.A. Kishore, M.V.A. Bianchi, C. Booten, J. Vidal, R. Jackson, Parametric and sensitivity analysis of a PCM-integrated wall for optimal thermal load modulation in lightweight buildings, Appl. Therm. Eng. 187 (2021) 116568, https://doi.org/10.1016/j.applthermaleng.2021.116568.
[21] N. Elawady, M. Bekheit, A.A. Sultan, A. Radwan, Energy assessment of a roof-integrated phase change materials, long-term numerical analysis with experimental validation, Appl. Therm. Eng. 202 (2022) 117773, https://doi.org/10.1016/j.applthermaleng.2021.117773.
[22] D. Li, C. Zhang, Q. Li, C. Liu, M. Arıcı, Y. Wu, Thermal performance evaluation of glass window combining silica aerogels and phase change materials for cold climate of China, Appl. Therm. Eng. 165 (2020) 114547, https://doi.org/10.1016/j.applthermaleng.2019.114547.
[23] O.A. Rehman, V. Palomba, D. Verez, E. Borri, A. Frazzica, V. Brancato, T. Botargues, Z. Ure, L.F. Cabeza, Experimental evaluation of different macro-encapsulation designs for PCM storages for cooling applications, J. Energy Storage 74 A 109359 (2023), https://doi.org/10.1016/j.est.2023.109359.
[24] E. Baccega, M. Bottarelli, S. Cesari, Addition of granular phase change materials (PCMs) and graphene to a cement-based mortar to improve its thermal performances, Appl. Therm. Eng. 229 (2023) 120582, https://doi.org/10.1016/j.applthermaleng.2023.120582.
[25] Y. Zhuang, Z. Liu, W. Xu, Effects of gradient porous metal foam on the melting performance and energy storage of composite phase change materials subjected to an internal heater: a numerical study and PIV experimental validation, Int. J. Heat Mass Transf. 183 (2022) 122081, https://doi.org/10.1016/j.ijheatmasstransfer.2021.122081.
[26] Y. Zhuang, H. Li, W. Xu, S.M. Huang, Experimental study on the melting performance of magnetic NEPCMs embedded in metal foam subjected to a non-uniform magnetic field, Sol. Energy Mater. Sol. Cells 250 (2023) 112077, https://doi.org/10.1016/j.solmat.2022.112077.
[27] H. Li, Y. Zhuang, J.C. Feng, Multi-scale experimental analysis on the coupled effects of ultrasonic field and magnetic field on the melting and energy storage performances for hybrid nano-enhanced phase change materials, J. Energy Storage 84 (2024) 110801, https://doi.org/10.1016/j.est.2024.110801.
[28] A. Palacios, M.E. Navarro, C. Barreneche, Y. Ding, Hybrid 3 in 1 thermal energy storage system – Outlook for a novel storage strategy, Appl. Energy 274 (2020) 115024, https://doi.org/10.1016/j.apenergy.2020.115024.
[29] M. Abdullah, N.A. Koushaeian, J.D. Shah, Chung, A review on thermochemical seasonal solar energy storage materials and modeling methods, Int. J. Air-Cond. Ref. 32 (2024) 1, https://doi.org/10.1007/s44189-023-00044-6.
[30] H. Huang, J. Lin, Q. Zhao, Z. Xie, Y. Xiao, Numerical model of PCM heat exchange based on dynamic boundary, Energy Rep. 8 (2022) 579–587, https://doi.org/10.1016/j.egyr.2022.05.214.
[31] J. Gasia, D. Groulx, N.H.S. Tay, L.F. Cabeza, Numerical study of dynamic melting enhancement in a latent heat thermal energy storage system, J. Energy Storage 31 (2020) 101664, https://doi.org/10.1016/j.est.2020.101664.
[32] D.L. Roux, S. Serra, S. Sochard, J.M. Reneaume, Dynamic simulation of a combined solar system including phase change material storage and its experimental validation, Renew. Energy 234 (2024) 121112, https://doi.org/10.1016/j.renene.2024.121112.
[33] C. Xu, Y. Xie, Z. Liao, Y. Ren, F. Ye, Numerical study on the desorption process of a thermochemical reactor filled with MgCl2·6H2O for seasonal heat storage, Appl. Therm. Eng. 146 (2019) 785–794, https://doi.org/10.1016/j.applthermaleng.2018.10.019.
[34] T.R.S. Gbenou, K. Wang, Study of a thermochemical heat storage reactor filled with polyaluminum sulfate for low-temperature application, Int. J. Energy Res. 2024 (2024) 7725377, https://doi.org/10.1155/2024/7725377.
[35] T. Shi, H. Xu, C. Qi, B. Lei, Y. Wu, C. Zhao, Multi-physics modeling of thermochemical heat storage with enhance heat transfer, Appl. Therm. Eng. 198 (2021) 117508, https://doi.org/10.1016/j.applthermaleng.2021.117508.

[36] Y. Zeng, R.J. Clark, Y. Galazutdinova, A. Odukomaiya, S. Al-Hallaj, M. Farid, S. Kaur, J. Woods, Open-Cycle Thermochemical Energy Storage for Building Space Heating: Practical System Configurations and Effective Energy Density, Appl. Energy 376 A (2024), https://doi.org/10.1016/j.apenergy.2024.124218.
[37] Y. Zhang, M. Hu, Z. Chen, Y. Su, S. Riffat, Performance study of a thermochemical energy storage reactor embedded with a microchannel tube heat exchanger for water heating, J. Energy Storage 78 (2024) 110043, https://doi.org/10.1016/j.est.2023.110043.
[38] Y. Zhang, M. Hu, Z. Chen, Y. Su, S. Riffat, Modelling analysis of a solar-driven thermochemical energy storage unit combined with heat recovery, Renew. Energy 206 (2023) 722–737, https://doi.org/10.1016/j.renene.2023.02.076.
[39] Z. Ma, H. Bao, A.P. Roskilly, Seasonal solar thermal energy storage using thermochemical sorption in domestic dwellings in the UK, Energy 169 (2019) 213–222, https://doi.org/10.1016/j.energy.2018.10.066.
[40] X. Yue, Y. Xu, X. Zhou, D. Xu, H. Chen, Study on the performance of a solar heating system with seasonal and cascade thermal-energy storage, Energies 15 (2022) 7733, https://doi.org/10.3390/en15207733.
[41] N. Mikos-Nuszkiewicz, P. Furmański, P. Łapka, A mathematical model of charging and discharging processes in a thermochemical energy storage reactor using the hydrated potassium carbonate as a thermochemical material, Energy 263 (2023) 125642, https://doi.org/10.1016/j.energy.2022.125642.
[42] L. Jiang, W. Liu, Y.C. Lin, R.Q. Wang, X.J. Zhang, M.K. Hu, Hybrid thermochemical sorption seasonal storage for ultra-low temperature solar energy utilization, Energy 239 B (2022) 213–222, https://doi.org/10.1016/j.energy.2021.122068.
[43] S. Mellouli, T. Alqahtani, F. Askri, S. Algarni, K. Ghachem, Parametric assessment of a hybrid heat storage unit based on paired metal hydrides and phase change materials, Appl. Therm. Eng. 226 (2023) 120257, https://doi.org/10.1016/j.applthermaleng.2023.120257.
[44] T. Alqahtani, Performance evaluation of a solar thermal storage system proposed for concentrated solar power plants, Appl. Therm. Eng. 229 (2023) 120665, https://doi.org/10.1016/j.applthermaleng.2023.120665.
[45] G. Zisopoulos, A. Nesiadis, K. Atsonios, N. Nikolopoulos, D. Stitou, A. Coca-Ortegón, Conceptual design and dynamic simulation of an integrated solar driven thermal system with thermochemical energy storage for heating and cooling, J. Energy Storage 41 (2021) 102870, https://doi.org/10.1016/j.est.2021.102870.
[46] ECHO – Efficient Compact modular tHermal energy stOrage system. https://echo-euproject.eu [Accessed 23rd July 2024].
[47] PCM Products Ltd. PlusICE Range. https://www.pcmproducts.net/files/PlusICE%20Range%202021-1.pdf [Accessed 23rd July 2024].
[48] PCM Products Ltd. https://www.pcmproducts.net [Accessed 23rd July 2024].
[49] Davis Instruments. Weather station Vantage Pro2. https://www.davisinstruments.com/vantage-pro2/ [Accessed 23rd July 2024].
[50] G. Emmi, E. Baccega, S. Cesari, E. Mainardi, M. Bottarelli, Energy analysis of multi-source heat pump system: A real case study application, Renew. Energy 221 (2024) 119708, https://doi.org/10.1016/j.renene.2023.119708.